Supplement of Atmos. Chem. Phys., 23, 12851–12865, 2023
https://doi.org/10.5194/acp-23-12851-2023-supplement

Atmospheric Chemistry and Physics
Open Access

Supplement of

Characterization of the nitrogen stable isotope composition (δ^{15}N) of ship-emitted NO_x

Zeyu Sun et al.

Correspondence to: Chongguo Tian (cgtian@yic.ac.cn)

The supplemental material has 16 pages and includes the following items:

Text S1. The reason for large variation of δ^{15}N–NO_x values within the same ship emissions under the same mode.

Text S2. The influence evaluation of the ship fuel type, the ship category, and the actual operational status of ships.

Text S3. Significance of ship-emitted δ^{15}N–NO_x values for accurate source apportionment of NO_x.

Table S1. Meteorological parameters during ship exhaust sampling (average values).

Table S2. Details on NO_x concentrations and δ^{15}N–NO_x values for collected ship.

Table S3. Statistics of δ^{15}N–NO_x values and ranges of variation for emissions from other sources.

Table S4. The accuracy of methods implemented to evaluate the impact degree of different factors on the variation in ship-emitted δ^{15}N–NO_x values.

Table S5. Mass-weighted δ^{15}N–NO_x values (‰) emitted from ships between 2001 and 2021.

Figure S1. The set up on the ship during sampling. The yellow arrow indicates the emission of exhaust from the ship.

Figure S2. δ^{15}N–NO_x values emitted from ships grouped by different fuels.

Figure S3. δ^{15}N–NO_x values emitted from ships grouped by different ship categories.

Figure S4. δ^{15}N–NO_x values emitted from ships grouped by different operational statuses.

Figure S5. Increase in mean squared error (%IncMSE) and increase in node purity (IncNodePurity) of selected factors for the δ^{15}N–NO_x values from ships calculated by random forest (RF).

Figure S6. Relative influence (%) of four selected factors on δ^{15}N–NO_x values from ships calculated by boosted regression trees (BRT).

Figure S7. Spatial distribution of annual NO_x emissions from coastal vehicles and offshore ships in China in 2017.

Figure S8. The age distribution of ships larger than 300 gross tonnage (GT) in the international merchant fleet during 2001 and 2021

Text S1. The reason for large variation of $\delta^{15}N–NO_x$ values within the same ship emissions under the same mode.

As shown in Table S2, significant differences in emissions under the same operating mode on the same ship were more often observed during hoteling and cruising conditions.

The hoteling mode typically occurs when a vessel is not departing from the port and not engaged in normal navigation operations, such as during cargo loading/unloading or while anchored awaiting further instructions. In the hoteling mode, although ME are usually shut down to reduce energy consumption and costs, there are still variations in emissions due to changes in the usage requirements of different onboard equipment. Cooper (2003) found that for approximately 5 min after arrival at the quayside, and approximately 15 min before departure, the power requirement for ships studied increased to 40–56% of the total installed AE power when bow and stern thrusters used for manoeuvring the ship were engaged. Additionally, cargo pumps used during the cargo handling process on bulk carriers and the refrigeration equipment for storing the catch on fishing vessels may lead to a significant increase in power demand during the hoteling mode.

In our study, the state in which the vessel operated at a higher speed (> 8 knots) was defined as the cruising mode. This mode exhibited a wide range of variation in ship speed. Moreover, ships often operate in cruise mode when navigating in open seas far from the coast and are more likely to encounter larger waves and swells. As a result, the engine load of a ship in cruise mode is more susceptible to fluctuations and changes compared to other operating modes (Huang et al., 2018), and consequently lead to variations in the NO_x measurement of exhaust samples collected during cruising conditions.

Text S2. The influence evaluation of the ship fuel type, the ship category, and the actual operational status of ships.

The statistics of $\delta^{15}N–NO_x$ values classified according to the ship fuel type, the ship category, and the actual operational status of ships are illustrated in Figures S2–S4. The influence of ship category on ship-emitted $\delta^{15}N–NO_x$ values primarily concerns engine types of different ships. For high-power engines, complete combustion of fuel raises the combustion temperature and the mixing time of fuel and air in the engine cylinder is longer, while the high oxygen content is also a dominant factor in NO_x generation (Zhang et al., 2018). Meanwhile, high temperature brings about more decomposition of NO in the engine. The decomposition reaction of ^{14}NO occurs faster than that of ^{15}NO since NO decomposition reactions are usually dynamically controlled, which leads to enrichment of ^{15}NO and an increase in $\delta^{15}N–NO_x$

values (Zong et al., 2020). This is to some extent consistent with our result that the mean values of δ^{15}N–NO_x emitted from the most powerful bulk carrier SH1 and the least powerful fishing vessel Y2 in this study are the largest and smallest among all sampled vessels, respectively, although they are influenced by many other factors. The minor influence of fuel type on δ^{15}N–NO_x values is due to the principle of thermally generated NO_x by internal combustion engines of ships as mentioned above (Goldsworthy, 2003). The operational condition of ships has the least effect on the variation in δ^{15}N–NO_x values. Previous studies have also elucidated that δ^{15}N–NO_x values emitted from motor vehicles were mainly altered during the period of cold or hot start and vary within a narrow range after 2 or 3 min of cold or hot start. The three operating modes of ships in this study should all be the state after a cold or hot start, so the minimum effect of the operating mode on the δ^{15}N–NO_x values is in accordance with the observations of motor vehicles (Walters et al., 2015a; Walters et al., 2015b; Zong et al., 2020).

Text S3. Significance of ship-emitted δ^{15}N–NO_x values for accurate source apportionment of NO_x.

With the transformation of the energy structure and the improvement of environmental standards, NO_x emissions from power plants as well as residential coal combustion have been increasingly restricted, and transportation has become one of the most widely concerned emission sources of NO_x in the atmosphere in recent years (Luo et al., 2019; Song et al., 2019; Zong et al., 2017). To assess the impact of transportation NO_x sources, we integrated vehicle emissions from coastal China and ship emissions from offshore China in 2017 reported in previous studies (the data are available on the website of http://meicmodel.org) and made the combined emission inventory of NO_x from ships and vehicles (Li et al., 2017; Liu et al., 2016). As shown in Figure S7, NO_x emissions are significantly higher in coastal areas, especially in some shipping-intensive ports in the Bohai Rim, Yangtze River Delta and Pearl River Delta, such as Qingdao, Shanghai and Guangzhou, indicating that the impact of ship emissions on atmospheric NO_x pollution cannot be ignored. In addition, it can be obtained in view of the previous analysis that the δ^{15}N–NO_x values of ship and motor vehicle emissions are distinctly different. Therefore, reliable δ^{15}N–NO_x values of ship emissions are essential for the accuracy of source apportionment when assessing atmospheric NO_x sources in coastal areas based on δ^{15}N methods.

Table S1. Meteorological parameters during ship exhaust sampling (average values).

vessel ID	temperature (°C)	wind speed (m s^{-1})	relative humidity (%)	sampling area	sampling period
SH1	24	2.8	66	Shanghai Port	2020/09/12–16
SH2	1	4.5	51	Yantai Port	2020/01/11–12
SH3	25	4.3	55	Dongying Port	2020/09/22
SH4	27	3.0	68	Weihai Port	2020/08/21
SH5	1	5.1	49	Yantai Port	2020/01/15
Y1	27	3.0	68	Weihai Port	2020/08/21
Y2	26	2.9	65	Weihai Port	2020/08/22
K1	27	3.3	63	Dandong Port	2021/07/08
KK1	25	4.1	58	Yantai Port	2021/09/13

Table S2. Details on NO_x concentrations and $\delta^{15}N$–NO_x values for collected ship exhaust (actual emissions after integration of main engine and auxiliary engine).

vessel ID	operational status	NO_x (ppm)		$\delta^{15}N$ (‰)		n (replicates)
		ave	std	ave	std	
SH1	maneuvering	144.0	66.1	−7.4	0.1	4
	cruising	114.4	93.9	−8.1	6.0	12
	total	129.2	80.0	−7.8	3.0	16
SH2	maneuvering	186.2	37.0	−11.4	0.0	6
	cruising	147.3	68.0	−10.6	1.9	12
	total	166.8	52.5	−11.0	0.9	18
SH3	hoteling	342.0	213.8	−31.0	2.0	6
	maneuvering	338.4	143.4	−30.5	1.3	6
	cruising	314.3	170.0	−29.7	5.9	12
	total	331.6	175.8	−30.4	3.1	24
SH4	hoteling	73.4	0.3	−10.0	0.0	2
	cruising	68.0	9.9	−15.7	2.0	2
	total	70.7	5.1	−12.9	1.0	4
SH5	hoteling	197.5	34.3	−18.8	4.7	4
	maneuvering	236.6	80.0	−13.3	10.3	2
	cruising	169.9	71.3	−24.3	10.3	4
	total	201.3	61.9	−18.8	8.4	10
Y1	hoteling	197.3	104.7	−24.2	4.6	4
	maneuvering	348.3	21.9	−17.5	9.5	2
	cruising	230.9	56.3	−21.1	5.2	6
	total	258.8	61.0	−20.9	6.4	12
Y2	hoteling	95.5	19.6	−34.3	1.1	4
	maneuvering	134.0	14.0	−32.7	3.1	2
	cruising	84.9	24.0	−33.9	1.3	6
	total	104.8	19.2	−33.6	1.8	12
K1	hoteling	19.4	9.9	−11.3	0.7	6

	cruising	10.9	0.5	−8.4	2.5	4
	total	15.1	5.2	−9.9	1.6	10
KK1	hoteling	22.2	0.4	−12.4	0.0	4
	maneuvering	52.4	17.7	−12.4	0.0	4
	cruising	61.2	27.2	−11.4	0.7	10
	total	45.2	15.1	−12.1	0.2	18

Table S3. Statistics of $\delta^{15}N–NO_x$ values and ranges of variation for emissions from other sources.

source	time	sampling[a]			^{15}N (‰)				n	ref	ave	std
					ave	std	min	max	(replicates)			
vehicle exhaust		individual vehicle tailpipes without TWC	the standard gas bubbler (KOH solution)	NO_x	3.7	0.3	3.4	3.9	3	(Moore, 1977)	0.46	6.93
		individual vehicle tailpipes without TWC	10 L glass tube ($NaOH/H_2O_2$ solution)	NO_x	−1.8					(Freyer, 1978)		
		individual vehicle tailpipes without TWC	17 L glass or polythene container ($NaOH/H_2O_2$ solution)	NO_x	−7.0	4.7	−13	−2	8	(Heaton, 1990)		
	1994/04/29 –08/19	roadside	the denuder system (CrO_3/H_3PO_4 solid oxidizer + KOH/guaiacol coating)	NO	3.1	5.4	−5	9.5	9	(Ammann et al., 1999)		
			the denuder system (KOH/guaiacol coating)	NO_2	5.7	2.8	1.6	10.1	9			
	2008/07−11	roadside	the Ogawa sampler (14.5 mm TEA coating filter)	NO_2	1.0	3.5	−5.1	7.3		(Redling et al., 2013)		
			the HNO_3 sampler (PTFE membrane + 47 mm nylon filter)	HNO_3	2.8		−1	3.1				
	2010/05–2011/05	outside and in the tunnel	the Ogawa sampler (14 mm TEA coating filter)	NO_2	15.0	1.6	10.2	17.0	22	(Felix and Elliott, 2014)		
			the HNO_3 sampler (2 µm 47 mm Teflon filter + 47 mm nylon filter)	HNO_3	5.7	2.8	0.9	11.1	15			
	2014/10/01 – 2015/05/01	individual vehicle tailpipes	evacuated 2 L borosilicate bottle (H_2SO_4/H_2O_2 solution)	NO_x	−11	6.62	−28.1	8.5	55	(Walters et al., 2015 b)		
	2014/06/20	individual vehicle	evacuated 2 L	NO_x	−3.0	7.2	−23.3	10.5	78	(Walt		

	–09/26	tailpipes	borosilicate bottle (H_2SO_4/H_2O_2 solution)							ers et al., 2015a)		
	2015/03–08	roadside	the gas-washing bottle ($KMnO_4$/NaOH solution)	NO_x			−9	−2	78	(Miller et al., 2017)		
	2019/04/16–27	individual vehicle tailpipes	the gas-washing bottle ($KMnO_4$/NaOH solution)	NO_x	−8.66	5.34	−18.8	6.43	61	(Zong et al., 2020)		
biogenic soil emission	1998/11/05–18	fertilized soil + the dynamic chamber	the trapping system (a molecular sieve 5A trap)	N_2O			−46	5	15	(Perez et al., 2001)		
		fertilized soil + the dynamic flow-through chamber	the denuder system (CrO_3/H_3PO_4 solid oxidizer + KOH/guaiacol coating)	NO	−32.3		−48.9	−19.9	24	(Li and Wang, 2008)		
	2010/06/19–07/22; 2011/06/2–06/19	fertilized soil + the feedlot flux chamber	the Ogawa sampler (14 mm TEA coating filter)	NO_2	−28.7	2.2	−30.8	−26.5	2	(Felix and Elliott, 2013, 2014)	−33.65	5.55
		re-wetted soil	9.5 mm i.d., ca. 240 cm length Teflon tubing (O_3) + 500 mL gas washing bottle (TEA solution)	NO	−43.0	9.3	−59.8	−23.4	35	(Yu and Elliott, 2017)		
	2016/05; 2017/05–06	fertilized no-till soil + the dynamic flux chamber	the gas-washing bottle ($KMnO_4$/NaOH solution)	NO_x	−30.6 (emission-weighted)		−44.2	14.0	37	(Miller et al., 2018)		

biomass burning	fall of 2016	stack and chamber fires	250 mL gas-washing bottle ($KMnO_4$/NaOH solution)	NO_x	1.0	4.1	−7.2	12	24	(Fibiger and Hastings, 2016)	−0.78	4.69
			the Nylasorb filter	HNO_3	6.3							
		chamber fires	the gas-washing bottle ($KMnO_4$/NaOH solution)	NO_x	1.1	3.1	−4.3	7.0	14	(Chai et al., 2019)		
			the Teflon particulate filter	pNO_3^-	−8.9	1.3	−10.6	−7.4	5			
	autumn	rural cooking stoves and open burning	evacuated 2 L borosilicate bottle (H_2SO_4/H_2O_2 solution)	NO_x	−3.8	4.2	−11.9	3.1	42	(Shi et al., 2022)		
	November	stack fires (residential use)	the gas-washing bottle ($KMnO_4$/NaOH solution)	NO_x	−0.4	2.4	−5.6	3.2	21	(Zong et al., 2022)		
coal combustion		coal-fired power stations	NaOH/H_2O_2 solution	NO_x	9.6	2.9	6	13	5	(Heaton, 1990)	8.84	7.93
		thermal/prompt NO_x		NO	−6.2	0.9				(Snape et al., 2003)		
	2009/05–2011/04	coal-fired power plants (in stack)	evacuated and purged flask (H_2SO_4/H_2O_2 solution) / NaOH/H_2O_2 solution	NO_x	14.6	4.5	9.0	25.6	38	(Felix et al., 2012)		
	2009/12/08		TEA solution	NO_2	10.1	0.6	9.5	10.7	4			
	November	residential coal combustion	the gas-washing bottle ($KMnO_4$/NaOH solution)	NO_x	16.1	3.3	11.7	19.7	7	(Zong et al., 2022)		

[a]The full names of the abbreviated forms and chemical formulas mentioned in the table are as follows: three-way catalytic (TWC), potassium hydroxide (KOH), sodium hydroxide (NaOH), hydrogen peroxide (H_2O_2), chromium trioxide (CrO_3), phosphoric acid (H_3PO_4), triethanolamine (TEA), nitric acid (HNO_3), poly tetra fluoroethylene (PTFE), sulfuric acid (H_2SO_4), potassium permanganate ($KMnO_4$), ozone (O_3).

Table S4. The accuracy of methods implemented to evaluate the impact degree of different factors on the variation in ship-emitted $\delta^{15}N$–NO_x values.

	mean error	root mean squared error	mean absolute error	mean percentage error	mean absolute percentage error
ctree	−1.61E−15	6.333	4.490	−21.806	53.884
cforest	−0.052	5.798	4.300	−19.875	49.085
rpart	−1.61E−15	6.333	4.490	−21.806	53.884
random forest	−0.071	4.358	2.934	−8.955	29.870

Table S5. Mass-weighted $\delta^{15}N$–NO_x values (‰) emitted from ships between 2001 and 2021.

year	mean	standard deviation	lower quartiles	upper quartiles
2001	−33.52	0.57	−33.90	−33.14
2002	−33.03	0.73	−33.49	−32.56
2003	−32.91	0.79	−33.42	−32.39
2004	−32.66	0.82	−33.16	−32.14
2005	−32.16	0.98	−32.77	−31.50
2006	−32.09	1.01	−32.73	−31.42
2007	−31.84	1.05	−32.53	−31.14
2008	−31.62	1.05	−32.32	−30.91
2009	−31.26	1.11	−32.04	−30.49
2010	−31.00	1.12	−31.74	−30.25
2011	−30.92	1.16	−31.66	−30.15
2012	−30.77	1.17	−31.53	−30.00
2013	−29.38	1.25	−30.17	−28.55
2014	−28.67	1.21	−29.43	−27.90
2015	−27.68	1.26	−28.45	−26.83
2016	−27.89	1.21	−28.65	−27.08
2017	−27.76	1.21	−28.50	−26.95
2018	−27.45	1.23	−28.20	−26.63
2019	−27.07	1.25	−27.85	−26.29
2020	−26.31	1.34	−27.16	−25.43
2021	−25.60	1.44	−26.49	−24.68
2022	−24.24	1.49	−25.19	−23.30
2023	−23.42	1.40	−24.41	−22.47
2024	−23.04	1.46	−24.02	−22.10
2025	−22.45	1.53	−23.54	−21.46
2026	−22.10	1.52	−23.13	−21.11
2027	−20.33	1.52	−21.40	−19.30
2028	−20.15	1.55	−21.22	−19.12
2029	−20.28	1.69	−21.41	−19.15
2030	−18.87	1.65	−20.01	−17.77
2031	−17.68	1.70	−18.89	−16.55

2032	−17.60	1.73	−18.72	−16.45
2033	−17.50	1.64	−18.56	−16.45
2034	−16.69	1.67	−17.80	−15.60
2035	−15.57	1.69	−16.75	−14.48
2036	−14.09	1.69	−15.16	−12.95
2037	−13.76	1.68	−14.92	−12.60
2038	−12.52	1.67	−13.74	−11.39
2039	−11.70	1.73	−12.87	−10.55
2040	−10.09	1.72	−11.30	−8.87
2041	−9.79	1.80	−11.06	−8.55
2042	−9.26	1.82	−10.60	−7.99
2043	−9.30	1.76	−10.55	−8.09
2044	−8.84	1.91	−10.07	−7.53
2045	−8.58	1.92	−9.87	−7.26
2046	−8.09	1.95	−9.44	−6.75
2047	−8.23	1.94	−9.50	−6.99
2048	−8.10	1.94	−9.46	−6.75
2049	−8.06	1.96	−9.32	−6.71
2050	−8.10	2.01	−9.54	−6.77
2051	−8.06	1.96	−9.33	−6.74
2052	−8.17	2.02	−9.52	−6.92

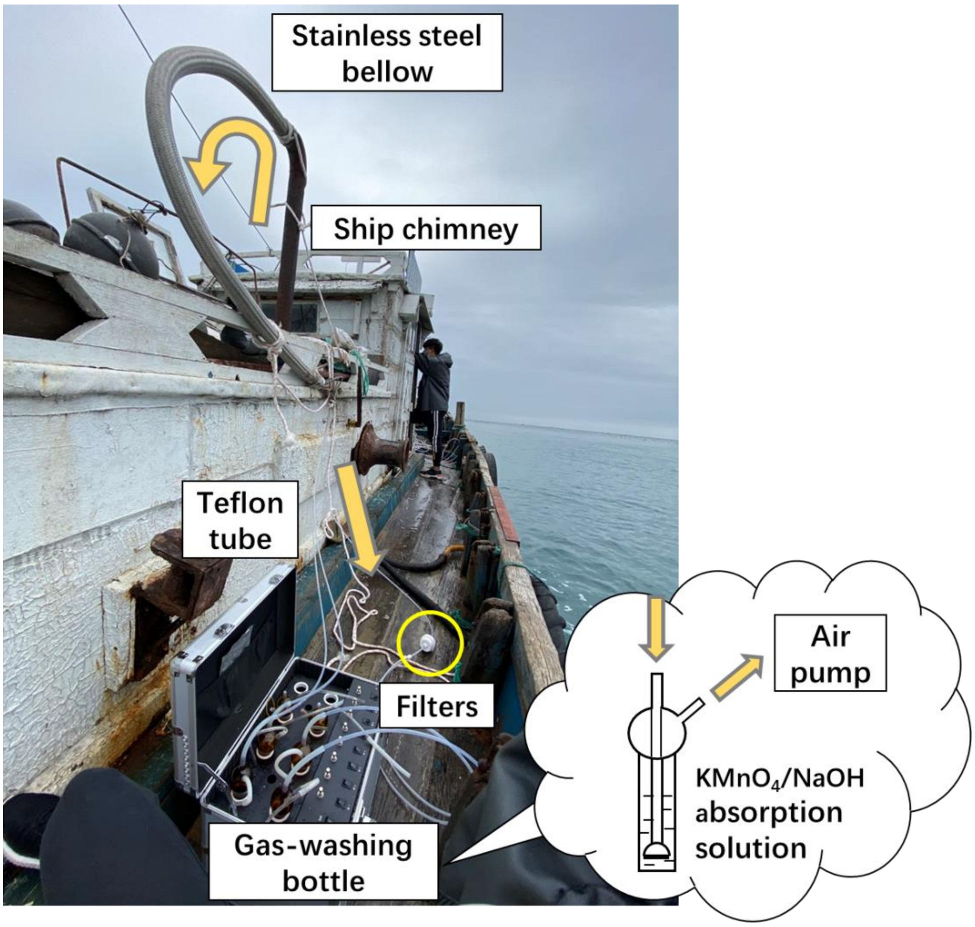

Figure S1. The set up on the ship during sampling. The yellow arrow indicates the emission of exhaust from the ship.

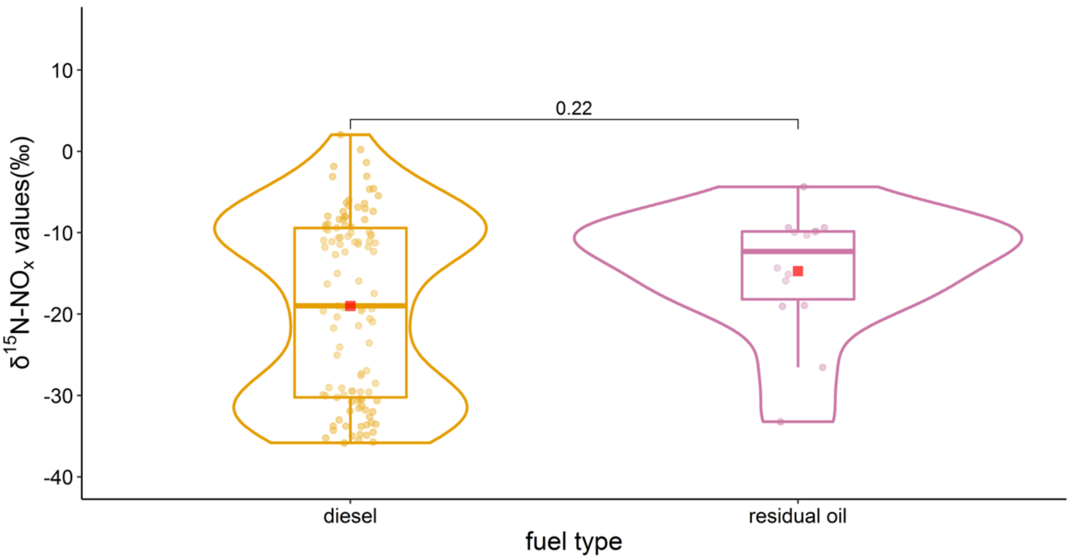

Figure S2. $\delta^{15}N–NO_x$ values emitted from ships grouped by different fuels. (red square, mean; center line, median; box bounds, upper and lower quartiles; whiskers, 1.5 times interquartile range; points, outliers; outer line, data distribution). The *p* value indicating the distinction between two selected groups is marked on the upper of the panel (the Mann–Whitney U test).

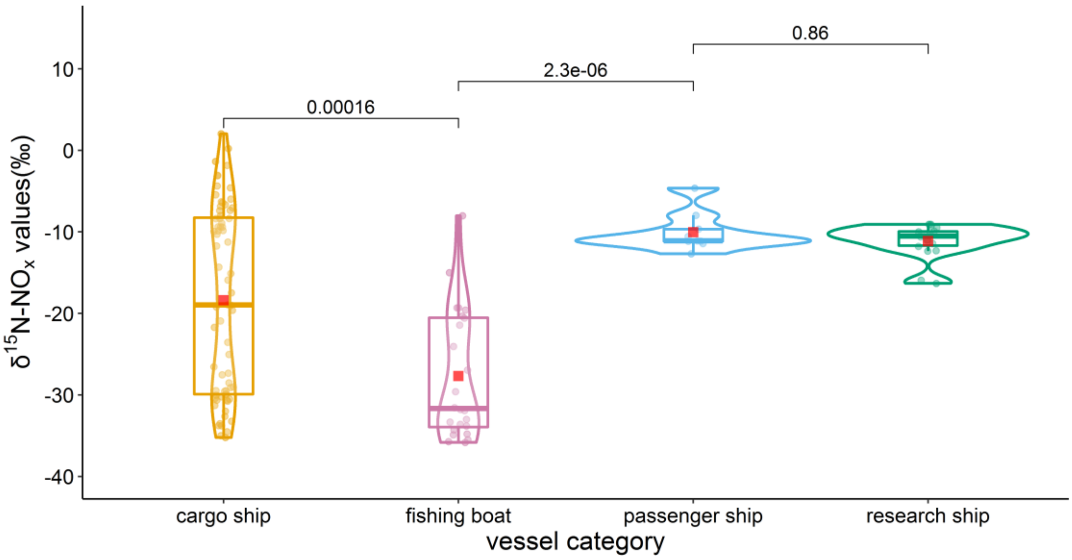

Figure S3. δ^{15}N–NO$_x$ values emitted from ships grouped by different ship categories. (red square, mean; center line, median; box bounds, upper and lower quartiles; whiskers, 1.5 times interquartile range; points, outliers; outer line, data distribution). The *p* values indicating the distinction between two selected groups are marked on the upper of the panel (the Mann–Whitney U test).

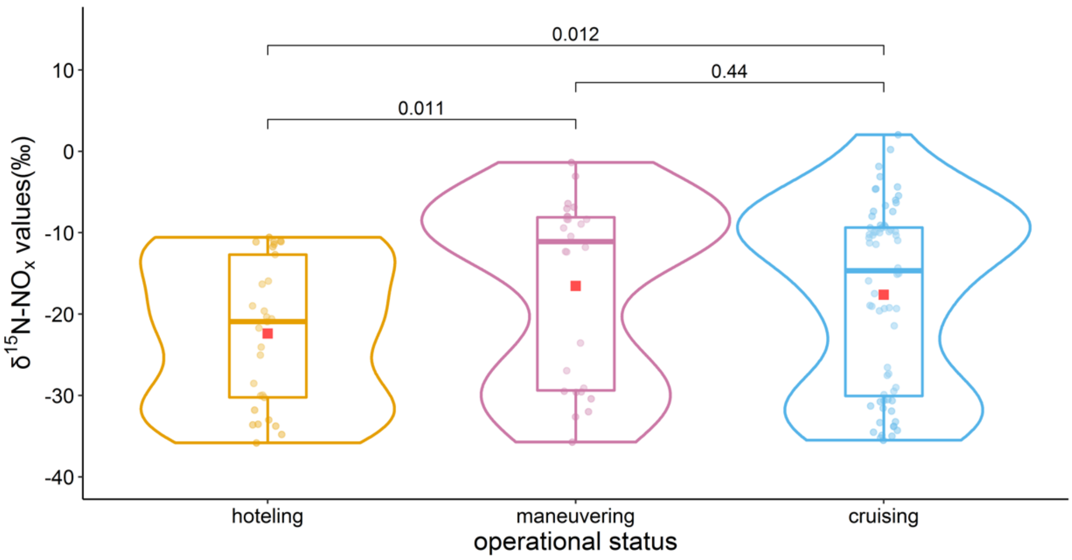

Figure S4. δ^{15}N–NO$_x$ values emitted from ships grouped by different operational statuses. (red square, mean; center line, median; box bounds, upper and lower quartiles; whiskers, 1.5 times interquartile range; points, outliers; outer line, data distribution). The *p* values indicating the distinction between two selected groups are marked on the upper of the panel (the Mann–Whitney U test).

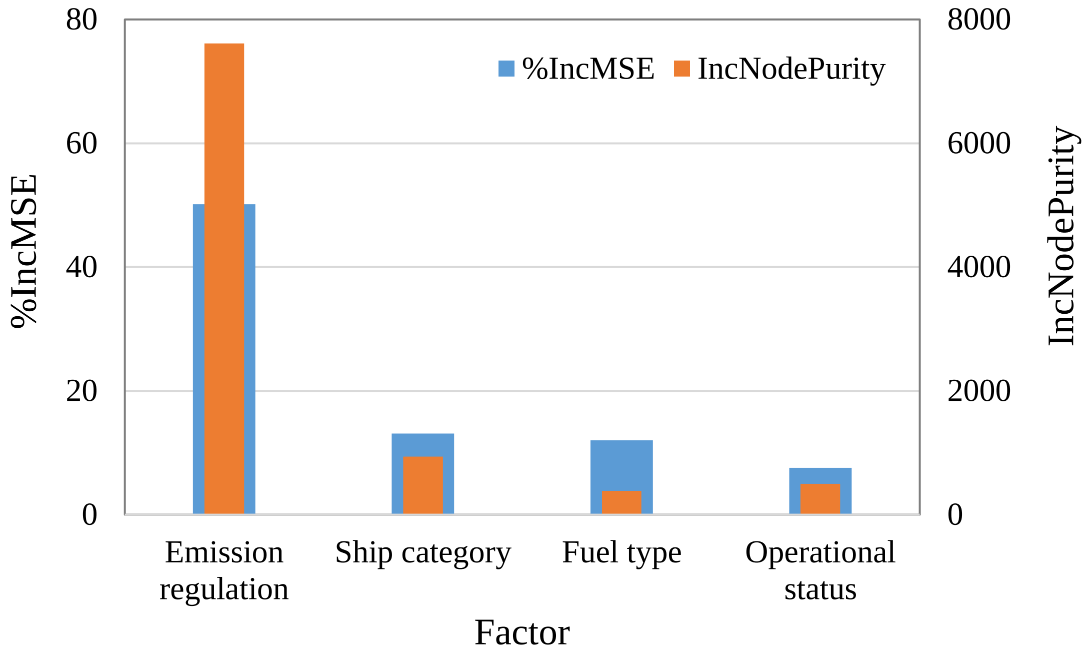

Figure S5. Increase in mean squared error (%IncMSE) and increase in node purity (IncNodePurity) of selected factors for the δ^{15}N–NO_x values from ships calculated by random forest (RF).

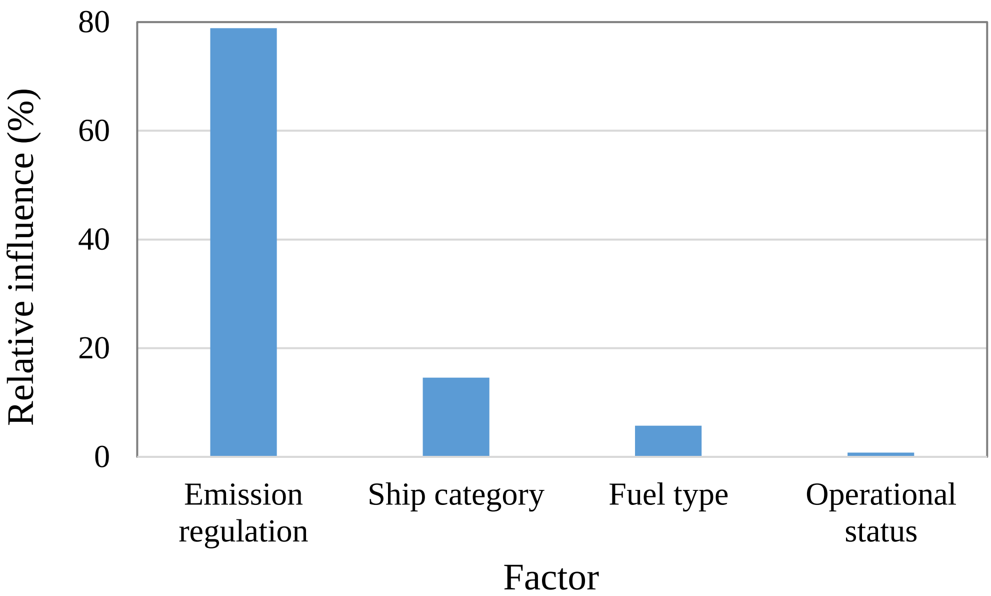

Figure S6. Relative influence (%) of four selected factors on δ^{15}N–NO_x values from ships calculated by boosted regression trees (BRT).

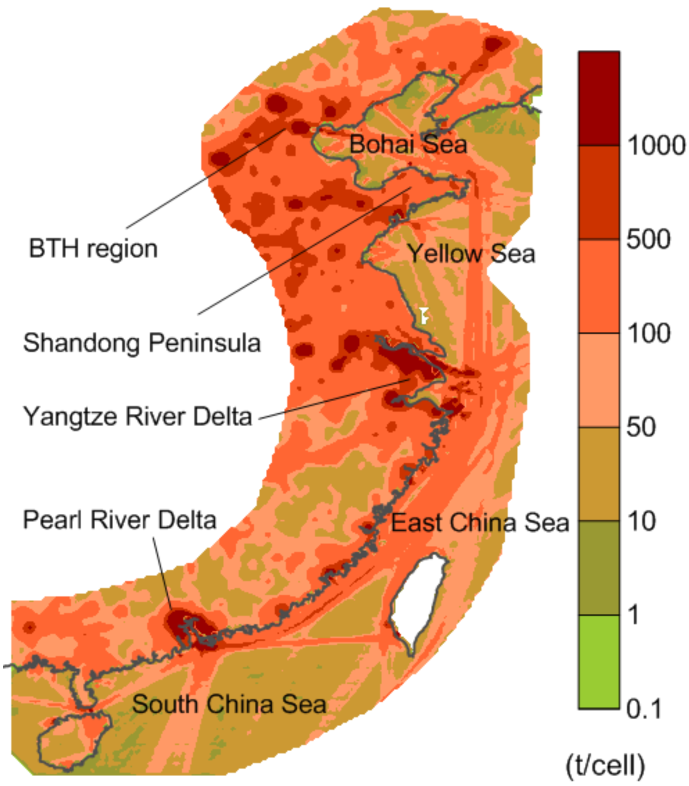

Figure S7. Spatial distribution of annual NO_x emissions from coastal vehicles and offshore ships in China in 2017 (a horizontal resolution of 0.1° × 0.1° latitude/longitude).

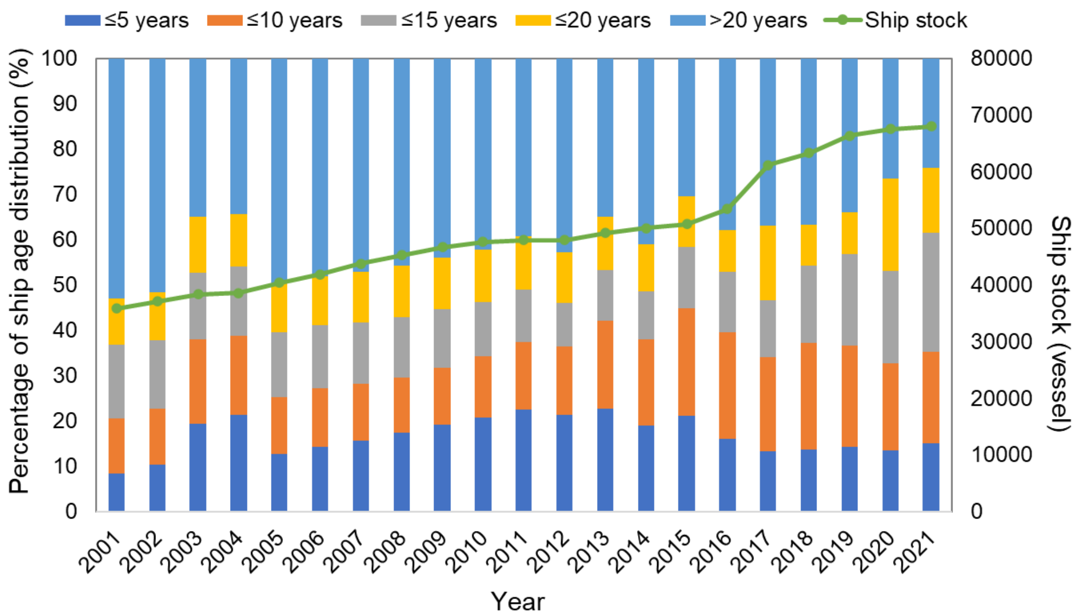

Figure S8. The age distribution of ships larger than 300 gross tonnage (GT) in the international merchant fleet during 2001 and 2021.

References

Ammann, M., Siegwolf, R., Pichlmayer, F., Suter, M., Saurer, M., and Brunold, C.: Estimating the uptake of traffic-derived NO_2 from ^{15}N abundance in Norway spruce needles, Oecologia, 118, 124-131, https://doi.org/10.1007/s004420050710, 1999.

Chai, J., Miller, D. J., Scheuer, E., Dibb, J., Selimovic, V., Yokelson, R., Zarzana, K. J., Brown, S. S., Koss, A. R., Warneke, C., and Hastings, M.: Isotopic characterization of nitrogen oxides (NO_x), nitrous acid (HONO), and nitrate (pNO_3^-) from laboratory biomass burning during FIREX, Atmos. Meas. Tech., 12, 6303-6317, https://doi.org/10.5194/amt-12-6303-2019, 2019.

Cooper, D. A.: Exhaust emissions from ships at berth, Atmos. Environ., 37, 3817-3830, https://doi.org/https://doi.org/10.1016/S1352-2310(03)00446-1, 2003.

Felix, J. D., Elliott, E. M., and Shaw, S. L.: Nitrogen isotopic composition of coal-fired power plant NO_x: Influence of emission controls and implications for global emission inventories, Environ. Sci. Technol., 46, 3528-3535, https://doi.org/10.1021/es203355v, 2012.

Felix, J. D. and Elliott, E. M.: The agricultural history of human-nitrogen interactions as recorded in ice core δN^{15}–NO_3^-, Geophys. Res. Lett., 40, 1642-1646, https://doi.org/10.1002/grl.50209, 2013.

Felix, J. D. and Elliott, E. M.: Isotopic composition of passively collected nitrogen dioxide emissions: Vehicle, soil and livestock source signatures, Atmos. Environ., 92, 359-366, https://doi.org/10.1016/j.atmosenv.2014.04.005, 2014.

Fibiger, D. L. and Hastings, M. G.: First measurements of the nitrogen isotopic composition of NO_x from biomass burning, Environ. Sci. Technol., 50, 11569-11574, https://doi.org/10.1021/acs.est.6b03510, 2016.

Freyer, H. D.: Seasonal trends of NH_4^+ and NO_3^- nitrogen isotope composition in rain collected at Julich, Germany, Tellus, 30, 83-92, https://doi.org/10.1111/j.2153-3490.1978.tb00820.x, 1978.

Goldsworthy, L.: Reduced kinetics schemes for oxides of nitrogen emissions from a slow-speed marine diesel engine, Energy Fuel., 17, 450-456, https://doi.org/10.1021/ef020172c, 2003.

Heaton, T. H. E.: $^{15}N/^{14}N$ ratios of NO_x from vehicle engines and coal-fired power stations, Tellus B, 42, 304-307, https://doi.org/10.1034/j.1600-0889.1990.t01-1-00009.x, 1990.

Huang, L., Wen, Y., Geng, X., Zhou, C., and Xiao, C.: Integrating multi-source maritime information to estimate ship exhaust emissions under wind, wave and current conditions, Transportation Research Part D: Transport and Environment, 59, 148-159, https://doi.org/https://doi.org/10.1016/j.trd.2017.12.012, 2018.

Li, D. and Wang, X.: Nitrogen isotopic signature of soil-released nitric oxide (NO) after fertilizer application, Atmos. Environ., 42, 4747-4754, https://doi.org/10.1016/j.atmosenv.2008.01.042, 2008.

Li, M., Liu, H., Geng, G. N., Hong, C. P., Liu, F., Song, Y., Tong, D., Zheng, B., Cui, H. Y., Man, H. Y., Zhang, Q., and He, K. B.: Anthropogenic emission inventories in China: a review, Natl. Sci. Rev., 4, 834-866, https://doi.org/10.1093/nsr/nwx150, 2017.

Liu, H., Fu, M., Jin, X., Shang, Y., Shindell, D., Faluvegi, G., Shindell, C., and He, K.: Health and climate impacts of ocean-going vessels in East Asia, Nat. Clim. Change, 6, 1037-+, https://doi.org/10.1038/nclimate3083, 2016.

Luo, L., Wu, Y., Xiao, H., Zhang, R., Lin, H., Zhang, X., and Kao, S.-j.: Origins of aerosol nitrate in Beijing during late winter through spring, Sci. Total Environ., 653, 776-782,

https://doi.org/10.1016/j.scitotenv.2018.10.306, 2019.
Miller, D. J., Wojtal, P. K., Clark, S. C., and Hastings, M. G.: Vehicle NO_x emission plume isotopic signatures: Spatial variability across the eastern United States, J. Geophys. Res.-Atmos., 122, 4698-4717, https://doi.org/10.1002/2016jd025877, 2017.
Miller, D. J., Chai, J., Guo, F., Dell, C. J., Karsten, H., and Hastings, M. G.: Isotopic composition of in situ soil NO_x emissions in manure-fertilizes cropland, Geophys. Res. Lett., 45, 12058-12066, https://doi.org/10.1029/2018gl079619, 2018.
Moore, H.: Isotopic composition of ammonia, nitrogen-dioxide and nitrate in atmosphere, Atmos. Environ., 11, 1239-1243, https://doi.org/10.1016/0004-6981(77)90102-0, 1977.
Perez, T., Trumbore, S. E., Tyler, S. C., Matson, P. A., Ortiz-Monasterio, I., Rahn, T., and Griffith, D. W. T.: Identifying the agricultural imprint on the global N_2O budget using stable isotopes, J. Geophys. Res.-Atmos., 106, 9869-9878, https://doi.org/10.1029/2000jd900809, 2001.
Redling, K., Elliott, E., Bain, D., and Sherwell, J.: Highway contributions to reactive nitrogen deposition: tracing the fate of vehicular NO_x using stable isotopes and plant biomonitors, Biogeochemistry, 116, 261-274, https://doi.org/10.1007/s10533-013-9857-x, 2013.
Shi, Y., Tian, P., Jin, Z., Hu, Y., Zhang, Y., and Li, F.: Stable nitrogen isotope composition of NO_x of biomass burning in China, Sci. Total Environ., 803, 149857, https://doi.org/10.1016/j.scitotenv.2021.149857, 2022.
Snape, C. E., Sun, C. G., Fallick, A. E., Irons, R., and Haskell, J.: Potential of stable nitrogen isotope ratio measurements to resolve fuel and thermal NO_x in coal combustion, Abstr. Pap. Am. Chem. Soc., 225, U843-U843, 2003.
Song, W., Wang, Y.-L., Yang, W., Sun, X.-C., Tong, Y.-D., Wang, X.-M., Liu, C.-Q., Bai, Z.-P., and Liu, X.-Y.: Isotopic evaluation on relative contributions of major NO_x sources to nitrate of $PM_{2.5}$ in Beijing, Environ. Pollut., 248, 183-190, https://doi.org/10.1016/j.envpol.2019.01.081, 2019.
Walters, W. W., Goodwin, S. R., and Michalski, G.: Nitrogen stable isotope composition ($\delta^{15}N$) of vehicle-emitted NO_x, Environ. Sci. Technol., 49, 2278-2285, https://doi.org/10.1021/es505580v, 2015a.
Walters, W. W., Tharp, B. D., Fang, H., Kozak, B. J., and Michalski, G.: Nitrogen isotope composition of thermally produced NO_x from various fossil-fuel combustion sources, Environ. Sci. Technol., 49, 11363-11371, https://doi.org/10.1021/acs.est.5b02769, 2015b.
Yu, Z. and Elliott, E. M.: Novel method for nitrogen isotopic analysis of soil-emitted nitric oxide, Environ. Sci. Technol., 51, 6268-6278, https://doi.org/10.1021/acs.est.7b00592, 2017.
Zhang, F., Chen, Y., Chen, Q., Feng, Y., Shang, Y., Yang, X., Gao, H., Tian, C., Li, J., Zhang, G., Matthias, V., and Xie, Z.: Real-world emission factors of gaseous and particulate pollutants from marine fishing boats and their total emissions in China, Environ. Sci. Technol., 52, 4910-4919, https://doi.org/10.1021/acs.est.7b04002, 2018.
Zong, Z., Wang, X., Tian, C., Chen, Y., Fang, Y., Zhang, F., Li, C., Sun, J., Li, J., and Zhang, G.: First assessment of NO_x sources at a regional background site in North China using isotopic analysis linked with modeling, Environ. Sci. Technol., 51, 5923-5931, https://doi.org/10.1021/acs.est.6b06316, 2017.
Zong, Z., Sun, Z., Xiao, L., Tian, C., Liu, J., Sha, Q., Li, J., Fang, Y., Zheng, J., and Zhang, G.: Insight into the variability of the nitrogen isotope composition of vehicular NO_x in China, Environ. Sci. Technol., 54, 14246-14253, https://doi.org/10.1021/acs.est.0c04749, 2020.
Zong, Z., Shi, X., Sun, Z., Tian, C., Li, J., Fang, Y., Gao, H., and Zhang, G.: Nitrogen isotopic composition of NO_x from residential biomass burning and coal combustion in North China, Environ. Pollut., 304, 119238-119238, https://doi.org/10.1016/j.envpol.2022.119238, 2022.